Supplementary Material

Supplementary Tables

Supplementary Table 1: Scanning parameters across fMRI experiments 1 to 4. MB=multi band (i.e. number of simultaneously acquired slices), S=sense factor. TR=repetition time in msec. Exp.=experiment.

		Groningen, NL, Exp. #1	**SPINOZA, Amsterdam, NL Exp. #2 & #4**				**SPINOZA, Amsterdam, NL Exp. #3**				
Anatomical acquisition parameters	Sequence	3D-spoiled T1-weighted	T1-weighted				T1-weighted				
	Slices	170	170				250				
	Resolution (mm)	256x256	240x222				256 x256				
	Field of view (mm)	232	240 x 240 x 170				240x256x250				
	Voxel size (mm)	1x1x1	1x1x1				1x1x1				
Functional acquisition parameters	Sequence	T2*-weighted	T2*-weighted				T2*-weighted				
	Slices		MB1S2 Exp#2&4	MB2S2 Exp#2	MB3S2 Exp#2	MB4S2 Exp#2	MB1S2	MB1S2	MB2S2	MB4S1.5	MB4S2
	N° of slices	41	40	40	39	40	44	36	44	44	44
	Echo time (ms)	28	27.6	27.6	27.6	27.6	30	30	30	30	30
	Thickness (mm)	3.5	3.5	3.5	3.5	3.5	2.7	3.3	2.7	2.7	2.7
	Gap (mm)	NO	0.34	0.34	0.34	0.34	0.27	0.33	0.27	0.27	0.27
	Flip angle	70	72.9	72.9	72.9	72.9	79	75	64	51	50
	Repetition time	2000	2060	1230	760	570	2450	2000	1220	700	630
	Resolution	64x62	80x157				80x78				
	Field of view (mm)	224	240 x 240 x 153.65				TR[2450,1220,700,630]=216x216x130.4 TR[2000]=240x240x130.3				
	Voxels size (mm)	3.5x3.5x3.5	3.0x3.0x3.0				TR[2450,1220,700,630]=2.7x2.7xx2.7 TR[2000]=3.0x3.0x3.3				
	Number of volumes acquired	345	360 Exp.#2; 325 and 326 for session 1 and 2 of Exp. #4				200	245	400	700	780

Supplementary Table 2: Schema of the temporal order of processing steps and bounding box size for the four processing pipelines testing the effect of different normalization parameters in Exp. #1. Each column details the order of processing steps used in a specific pipeline. All pipelines start with core preprocessing including: centering of the anatomical image to the anterior commissure, slice timing, realignment of all EPI images to one another. Finally, the T1 image is coregisted to the mean EPI image. Only then do the different pipelines start to differ. The acronym of the different pipelines is constructed using the following elements. WB: whole-brain. Cereb: Cerebellum specific analysis. GLM: general linear model, referring to the first level of analysis. SUIT: spatially unbiased atlas template. MNI: MNI brain template. norm: normalization.

WB_MNInorm_GLM	WBcut_MNInorm_GLM	Cereb_GLM_SUITnorm	WB_GLM_MNInorm
slice timing	slice timing	slice timing	slice timing
EPI realignment	EPI realignment	EPI realignment	EPI realignment
T1-EPI coregistration	T1-EPI coregistration	T1-EPI coregistration	T1-EPI coregistration
whole-brain normalization **large** box	**whole-brain normalization** **small** box	GLM	GLM
smoothing	smoothing	**cerebellar normalization** **large** box	**whole-brain normalization** **large** box
GLM	GLM	smoothing	smoothing

Supplementary Table 3. Cerebellar activations to ActionOBS-CtrlOBS for the WB_MNInorm_GLM and the Cereb_GLM_SUITnorm pipelines. Regions with ActionOBS-CtrlOBS≥5.4. Only clusters with minimum 10 voxels are reported. Clusters are described using SPM Anatomy Toolbox. From left to right: the cluster size in number of voxels, the number of voxels falling in a cyto-architectonic area, the percentage of the cluster that falls in the cyto-architectonic area, the hemisphere (L=left; R=right), the name of the cyto-architectonic area when available or the anatomical description, the percentage of the area that is activated by the cluster, the t values of the peaks associated with the cluster followed by their MNI coordinates in mm. See Supplementary methods 1.1 and Supplementary results 1.1 for additional details.

Cluster size	# Voxels in cyto	% Cluster	Hem	Cyto or anatomical description	% Area	Peak Information			
						T	x	y	z
Exp. #1,WB_MNInorm_GLM pipeline, ActionOBS-CtrlOBS p_{FWE}<0.05, t=5.8, min. 10 voxels									
138	130.8	94.7	R	Lobule VI (Hem)	7.2	9.41	30	-56	-24
						8.13	32	-50	-30
						6.96	38	-48	-28
						6.95	30	-46	-24
100	66.6	66.6	L	Lobule VIIIa (Hem)	8.8	7.48	-26	-60	-52
						6.41	-20	-64	-56
	27.8	27.8	L	Lobule VIIb (Hem)	4.1	7.68	-12	-74	-48
	4.5	4.5	L	Lobule VIIIb (Hem)	0.7				
94	83	88.3	R	Lobule VIIb (Hem)	12.7	9.28	18	-78	-52
						9.13	14	-76	-48
						8.63	16	-74	-46
79	77.5	98.1	L	Lobule VI (Hem)	4.1	12.22	-28	-54	-24
						6.24	-34	-52	-28
47	43.1	91.8	R	Lobule VI (Hem)	2.4	10.13	22	-72	-22
47	45.8	97.3	R	Lobule VIIIa (Hem)	6.3	7.84	24	-64	-54
						7.03	30	-60	-52
						6.5	18	-68	-54
Exp. #1, Cereb_GLM_SUITnorm pipeline, ActionOBS-CtrlOBS p_{FWE}<0.05, t=5.4, min. 10 voxels									
214	199.1	93	R	Lobule VI (Hem)	11	9.18	30	-56	-24
						8.25	22	-72	-22
						7.48	32	-52	-28
						6.72	26	-66	-20
159	110.4	69.4	L	Lobule VIIIa (Hem)	14.5	7.97	-26	-58	-54
						7.62	-24	-60	-52
						7.11	-20	-62	-58
	25.4	16	L	Lobule VIIb (Hem)	3.7	8.35	-16	-74	-52
						8.05	-14	-72	-48
	21.1	13.3	L	Lobule VIIIb (Hem)	3.5	8.44	-20	-60	-48
118	97.4	82.5	R	Lobule VIIb (Hem)	14.9	8.35	16	-74	-46
						7.93	14	-76	-52
						7.78	12	-76	-48
						7.68	18	-78	-54
	14.1	12	R	Lobule VIIIa (Hem)	1.9				
101	99	98	L	Lobule VI (Hem)	5.3	11.04	-28	-54	-24
						7.35	-24	-56	-28
						6.08	-28	-60	-22
72	65.6	91.1	R	Lobule VIIIa (Hem)	9	8.17	24	-64	-54
						7.56	26	-60	-56
Exp. #1, WB_GLM_MNInorm pipeline, ActionOBS-CtrlOBS p_{FWE}<0.05, t=5.4, min. 10 voxels									
102	91.4	89.6		Lobule VIIb (Hem)	14	9.3	18	-78	-52
						8.97	14	-76	-48
						8.52	16	-74	-46
101	96.3	95.3		Lobule VI (Hem)	5.3	9.3	30	-56	-24
						8.06	32	-50	-30
						7.1	36	-50	-30
						6.91	30	-46	-24
94	61.6	65.6	left	Lobule VIIIa (Hem)	8.1	7.52	-26	-60	-52
					4	6.4	-26	-64	-56
					0.7	6.16	-22	-64	-56
	27	28.7	left	Lobule VIIb (Hem)		7.74	-14	-74	-48
73	71.5	97.9	left	Lobule VI (Hem)	3.8	12.49	-28	-54	-24
42	41.5	98.8		Lobule VIIIa (Hem)	5.7	7.74	24	-64	-54
						7.02	30	-60	-52
						6.54	18	-68	-54
39	35.9	92		Lobule VI (Hem)	2	10.13	22	-72	-22
						7	26	-66	-20

Supplementary Table 4. Number of activated cerebellar voxel. Median of activated voxels for the ActionOBS-ActionCtrl contrast for each experiment individually (Exp1-3) and when considered as a group (All; N=79), for each of the four anatomically defined cerebellar clusters identified at the group level (but separately for each hemisphere: L, left; R, right). Results are also reported for the whole cerebellum (Cereb), and for cortical areas activated by the same contrast and of similar volume (PF L, PF R, BA44L, BA44R). Percentage of participants having no voxels (% zeros) in any of the region of interest, and the percentage of those having at more than 10 voxels (%>10) are also reported. The size, in number of voxels, of each ROI is indicated under the ROI name in the first line (Area size).

		V L	V R	VI L	VI R	VIIIa/ VIIb L	VIIIa/ VII R	Cereb	PF L	PF R	BA44 L	BA44 R	BA1/2 L	BA1/2 R
Area size		732	786	2085	2041	1640	1588	21127	2205	2337	869	607	1101	1349
median	**Exp1**	0	0	14	47	4	5	208	517	373	115	41	115	501
	Exp2	0	0	4	10	9	54	186	244	146	89	20	88	254
	Exp3	0	0	67	50	8	82	384	450	282	91	72	91	705
	All	0	0	14	31	7	44	224	379	282	92	30	92	485
% zeros	**Exp1**	87.1	77.4	25.8	25.8	45.2	29.0	12.9	0.0	0.0	12.9	19.4	12.90	0.0
	Exp2	80.0	76.0	32.0	24.0	28.0	12.0	0.0	0.0	8.0	4.0	20.0	4.00	4.0
	Exp3	65.2	73.9	17.4	21.7	26.1	17.4	0.0	8.7	13.0	13.0	13.0	13.04	4.4
	All	78.5	75.9	25.3	24.1	34.2	20.3	5.1	2.5	6.3	10.1	17.7	10.13	2.5
% >10	**Exp1**	6.5	16.1	51.6	58.1	38.7	45.2	77.4	100.0	93.6	83.9	67.7	83.87	100.0
	Exp2	8.0	12.0	40.0	48.0	48.0	84.0	88.0	96.0	84.0	92.0	60.0	92.00	92.0
	Exp3	13.0	17.4	60.9	69.6	47.8	73.9	95.7	91.3	82.6	73.9	78.3	73.91	91.3
	All	8.7	15.2	50.6	58.2	44.3	65.8	86.1	96.2	87.3	83.5	68.4	83.54	94.9

Supplementary Table 5. Whole brain activations to ActionOBS-CtrlOBS. Regions with ActionOBS-CtrlOBS≥2.48 (p_{FWE}<0.05) across Exp1-3 (global null from the one-way ANOVA with the three experiments as factors). Only clusters with minimum 10 voxels are reported (k ≥10). Conventions as in Supplementary Table 3.

Cluster Size	#Voxels in Cyto	% Cluster	Hem	Cyto or Anatimical description	% Area	Peak Information			
						T	x	y	z
ActionOBS-CtrlOBS, pFWE<0.05, t=2.48, k≥10									
3665	482.3	13.2	L	Area 2	91.6	9.97	-50	-26	38
						9.78	-44	-28	40
						8.19	-36	-38	52
						7.55	-38	-40	60
	466	12.7	L	Area PFt (IPL)	79.9	9.6	-56	-20	28
	271.9	7.4	L	Area 5L (SPL)	39.2	4.71	-16	-54	68
	239.1	6.5	L	Area 3b	42.4				
	221.6	6	L	Area 7A (SPL)	17.7	5.33	-20	-56	60
						4.86	-22	-58	54
	160.6	4.4	L	Area 1	28.2	7.52	-58	-20	40
	126.6	3.5	L	Area OP1 [SII]	34	5.52	-56	-18	18
	120.8	3.3	L	Area 7PC (SPL)	70.8	6.69	-30	-48	60
	109	3	L	Area PFop (IPL)	49.1				
	63.3	1.7	L	Area hIP3 (IPS)	13.8				
	63	1.7	L	Area OP4 [PV]	17.4				
	51.8	1.4	L	Area 3a	18				
	36.1	1	L	Area PF (IPL)	6.9				
	19.6	0.5	L	Area hIP2 (IPS)	8.7				
	15.6	0.4	L	Area hOc4d [V3A]	2.7				
	9.3	0.3	L	Area 4a	1				
	8.4	0.2	L	Area 4p	2.6				
	2.1	0.1	L	Area TE 3	0.2				
	2	0.1	L	Area TE 1.0	1.6				
	1.8	0	L	Area OP3 [VS]	1.2				
	1	0	L	Area hIP1 (IPS)	0.3				
	0.9	0	L	Area 7P (SPL)	0.3				
	0.6	0	L	Area PFcm (IPL)	0.2				
2678	587.4	21.9	R	Area 2	90.3	6.57	44	-28	44
						6.56	32	-42	56
						6.55	38	-36	52
						6.46	30	-42	60
						6.36	34	-38	56
						6.07	40	-42	60
	328.1	12.3	R	Area 3b	52.2	7.57	52	-18	36
						6.68	40	-28	44
	324.4	12.1	R	Area 1	46.2	6.49	56	-18	42
	299.9	11.2	R	Area PFt (IPL)	71.9				
	205	7.7	R	Area 7PC (SPL)	45.1				
	113.4	4.2	R	Area PFop (IPL)	49.6	7.76	58	-16	28
	104.1	3.9	R	Area hIP3 (IPS)	22.8				
	91.5	3.4	R	Area OP1 [SII]	23.4				
	68.8	2.6	R	Area 5L (SPL)	9.4				
	57.5	2.1	R	Area 7A (SPL)	7.4				
	57.4	2.1	R	Area 3a	28.5	6.85	34	-30	44
	36.9	1.4	R	Area OP4 [PV]	11.8				
	33.4	1.2	R	Area 4p	10.7				
	31.3	1.2	R	Area PF (IPL)	4.6				
	18.5	0.7	R	Area 4a	1.7				
	9.3	0.3	R	Area hIP2 (IPS)	4.4				
	2.8	0.1	R	Area PFm (IPL)	0.4				
	1	0	R	Area TE 1.0	0.7				
	0.5	0	R	Area TE 3	0				
1389	291.6	21	L	Lobule VI (Hem)	15.6	5.82	-30	-50	-22
						5.54	-32	-48	-26
						4.29	-18	-68	-22
	177.9	12.8	L	Area FG4	30.1				
	168.1	12.1	L	Area FG3	20.3				
	61.1	4.4	L	Area hOc4la	7.2				
	36.6	2.6	L	Area hOc5 [V5/MT]	45.6				
	26.3	1.9	L	Area FG2	5.1				
	8.9	0.6	L	Area FG1	3.5				
	5.5	0.4	L	CA1 (Hippocampus)	2.5				
	3.9	0.3	L	Lobule VIIa crusI (Hem)	0.1	3.24	-44	-54	-30
	3	0.2	L	Lobule V (Hem)	0.4				
				Middle Temporal gyrus		6.02	-48	-60	-4
				Inferior Temporal Gyrus		5.63	-46	-66	-6
				Area FG3		5.09	-48	-54	
						5.08	-46	-56	-12
						3.11	-44	-52	-26

				Area FG4		4.53	-32	-38	-20
				Fusiform Gyrus		4.16	-32	-30	-22
1196	335	28	L	Area 44	38.2	4.66	-58	10	16
						4.65	-54	10	16
	7.8	0.6	L	Area OP3 [VS]	5.5				
	0.8	0.1	L	Area Ig2	0.6				
	0.4	0	L	Area OP4 [PV]	0.1				
	0.1	0	L	Area TE 1.2	0.1				
			L	Insula Lobe		8.43	-40	-4	10
			L	Precentral Gyrus		6.89	-54	4	36
988	446	45.1	R	Lobule VI (Hem)	24.7	6.92	30	-52	-24
						4.55	20	-68	-22
	324.4	32.8	R	Area FG4	66.3	5.06	28	-44	-18
						4.09	30	-32	-22
						4.07	30	-56	-12
	26.1	2.6	R	Area FG1	10.5				
	25	2.5	R	Area FG3	3.8				
	6.8	0.7	R	Lobule V (Hem)	0.8				
	6.1	0.6	R	Area FG2	1.9	2.91	42	-58	-26
	5.4	0.5	R	Subiculum	1.4				
	1.8	0.2	R	Lobule VIIa crusI (Hem)	0.1				
	1.6	0.2	R	CA1 (Hippocampus)	0.6				
	0.3	0	R	Area hOc3v [V3v]	0				
			R	ParaHippocampal Gyrus		3.29	34	-18	-26
						3.25	32	-22	-24
722	395.5	54.8	L	Area hOc4lp	46.2	4.63	-26	-96	-6
						4.58	-30	-84	10
						4.31	-38	-84	14
						4.25	-30	-94	-6
						3.91	-32	-88	-4
	61.1	8.5	L	Area hOc3v [V3v]	6.6	3.74	-20	-92	-14
	54.4	7.5	L	Area hOc4la	6.4				
	17.6	2.4	L	Area hOc4v [V4(v)]	2.4				
	7.3	1	L	Area hOc4d [V3A]	1.3				
	1.4	0.2	L	Area hOc3d [V3d]	0.1				
	0.9	0.1	L	Area hOc5 [V5/MT]	1.1				
	0.6	0.1	L	Area PGp (IPL)	0.1				
681	241.8	35.5	R	Area hOc4lp	43.2	4.88	34	-86	4
						4.58	38	-82	10
						4.12	32	-88	14
	77.3	11.3	R	Area hOc3v [V3v]	9.1	4.87	26	-92	-6
	43.1	6.3	R	Area hOc4la	4.9				
	16.1	2.4	R	Area hOc1 [V1]	0.8				
	11.8	1.7	R	Area hOc4v [V4(v)]	1.9				
	3	0.4	R	Area hOc4d [V3A]	0.7				
	2.1	0.3	R	Area PGp (IPL)	0.2				
	1.3	0.2	R	Area hOc3d [V3d]	0.2				
	0.5	0.1	R	Area hOc2 [V2]	0				
			R	Middle Occipital Gyrus		4.69	32	-82	8
621	n.p.m.		L	Superior Frontal Gyrus		6.12	-24	-8	60
			L	Precentral Gyrus		4.64	-34	-8	60
			L	Middle Frontal Gyrus		3.87	-24	2	60
448	36.6	8.2	R	Area FG3	5.6				
	22	4.9	R	Area FG2	6.8				
	10.9	2.4	R	Area hOc4la	1.2				
	1.9	0.4	R	Area hOc5 [V5/MT]	3.2				
	1.6	0.4	R	Area FG1	0.7				
			R	Inferior Temporal Gyrus		5.7	50	-62	-8
						5.3	48	-54	-10
429	134	31.2	R	Lobule VIIIb (Hem)	18.7	4.28	26	-50	-50
						4.21	18	-52	-54
	128.9	30	R	Lobule VIIIa (Hem)	17.7	5.85	12	-74	-50
						5.07	24	-58	-54
						4.75	26	-56	-52
	66.1	15.4	R	Lobule VIIb (Hem)	10.1	6.71	18	-72	-52
	40.8	9.5	R	Lobule IX (Hem)	5.8				
	22.5	5.2	R	Lobule VIIIa (Verm)	10.7				
	1.4	0.3	R	Lobule VIIIb (Verm)	1.9				
373	34	9.1	R	Area OP3 [VS]	16.2				
	4.9	1.3	R	Area Ig2	3.1				
			R	Insula Lobe		7.7	38	0	12
						6.71	40	-2	0
366	n.p.m		R	Superior Frontal Gyrus		6.67	28	-6	60
						2.94	16	-12	62
360	13.5	3.8	R	Area 33	6.2				

	5.4	1.5	L	Area 33	2.5				
			L	MCC		4.81	-2	4	38
			L	ACC		4.35	-2	8	30
			L	Posterior-Medial Frontal		4.32	-4	0	50
359	172.8	48.1	R	Area 44	28.8	6.96	58	8	26
	7.4	2.1	R	Area 45	0.7				
208	0.3	0.1	R	Area hOc4d [V3A]	0.1				
			R	Superior Occipital Gyrus		4.09	28	-74	34
194	90.1	46.5	L	Lobule VIIIa (Hem)	11.8	5.66	-18	-68	-48
						3.86	-26	-52	-50
	58.6	30.2	L	Lobule VIIIb (Hem)	9.7	4.56	-20	-58	-52
	17.5	9	L	Lobule VIIb (Hem)	2.6				
	2.1	1.1	L	Lobule VIIIa (Verm)	1.4				
	0.1	0.1	L	Lobule IX (Hem)	0				
165	0.5	0.3	L	Area 5Ci (SPL)	0.4				
			L	MCC		4.79	-12	-24	40
105	67.8	64.5	L	Thal: Prefrontal	10.7	4.22	-14	-22	8
	18	17.1	L	Thal: Parietal	5.7				
	12	11.4	L	Thal: Temporal	2.3	2.66	-16	-32	0
	3.4	3.2	L	Thal: Premotor	2.8				
	3.4	3.2	L	Thal: Visual	3.8				
	0.5	0.5	L	Thal: Motor	1				
50	34.1	68.3	R	Thal: Parietal	10.2	3.33	16	-22	6
	7.8	15.5	R	Thal: Prefrontal	1.4				
	5.6	11.3	R	Thal: Somatosensory	6.9				
	1.5	3	R	Thal: Premotor	1.1				
	0.8	1.5	R	Thal: Visual	1.8				
	0.3	0.5	R	Thal: Motor	0.6				
44	n.p.m.		L	IFG (p. Triangularis)		3.23	-42	36	10
22	2.4	10.8	R	Area 45	0.2				
			R	IFG (p. Triangularis)		3.18	48	36	8
13	8.1	62.5	R	Lobule VIIIa (Verm)	3.9				
	4.9	37.5	R	Lobule VIIb (Verm)	14.9	3.05	4	-72	-34
12	3.5	29.2	L	BF (Ch 4)	7	2.76	-22	0	-12
	0.1	1	L	Amygdala (CM)	0.3				
			L	Putamen		2.59	-24	0	-6

Supplementary Table 6. Cerebellar activations to the weight discrimination task. Results are shown at $p_{FWE}<0.05$ with cluster size >10 voxels. Conventions as in Table 3.

Cluster size	#Voxels in cyto	% Cluster	Hem	Cyto or anatomical description	% Area	Peak Information			
						T	x	y	z
Sleeve OR NoSleeve, pFWE<0.05, t>2.8									
6254	898.6	14.4	L	Lobule VI (Hem)	48	7.02	-8	-76	-28
						6.87	-6	-78	-24
						6.22	-30	-58	-30
	797.1	12.7	R	Lobule VI (Hem)	44.2	6.86	28	-64	-24
						6.37	36	-46	-32
	793.3	12.7	L	Lobule VIIa crusI (Hem)	26.1	7.09	-36	-64	-30
						7.07	-40	-64	-32
						6.33	-44	-58	-28
	573.9	9.2	R	Lobule VIIa crusI (Hem)	17.7				
	373	6	L	Lobule VIIIa (Hem)	49	6.73	-8	-72	-46
	296.8	4.7	L	Lobule VIIb (Hem)	43.7				
	230.3	3.7	R	Lobule VIIIa (Hem)	31.7				
	199.9	3.2	L	Lobule VIIa crusII (Hem)	12.2				
	169.6	2.7	R	Lobule VIIb (Hem)	25.9	6.09	30	-64	-50
	146.1	2.3	R	Lobule VIIIa (Verm)	69.7				
	132.6	2.1	L	Lobule VIIIb (Hem)	21.9				
	130.8	2.1	L	Lobule VIIIa (Verm)	88.3				
	121.3	1.9	L	Lobule IX (Hem)	19.5				
	73.1	1.2	R	AreaFG3	11.2				
	72.6	1.2	R	Lobule VIIa crusII (Hem)	5.1				
	69.4	1.1	R	Lobule VIIIb (Hem)	9.7				
	64.4	1	L	Lobule VI (Verm)	30.7				
	59.6	1	R	Lobule VI (Verm)	25.7				
	46.5	0.7	R	Area FG4	9.5				
	46.3	0.7	R	Lobule IX (Hem)	6.6				
	42.5	0.7	R	Area FG2	13.1				
	38.1	0.6	R	Area FG1	15.3				
	36	0.6	L	Lobule VIIb (Verm)	117.6				
	33.6	0.5	L	Lobule VIIIb (Verm)	54.5				
	32.5	0.5	R	Lobule VIIIb (Verm)	45.1				
	31.9	0.5	R	Lobule VIIb (Verm)	97.3				
	24.3	0.4	L	AreaFG3	2.9				
	17.5	0.3	R	Lobule VIIa crusII (Verm)	30.8				
	16.9	0.3	R	Area hOc4v [V4(v)]	2.7	6.23	36	-74	-22
	14.3	0.2	L	Area FG2	2.8				
Sleeve OR NoSleeve, masked with Exp. #1-3, pFWE<0.05, t>2.4									
585	451.8	77.2	R	Lobule VI (Hem)	25	6.95	28	-64	-24
						5.83	34	-46	-32
						5.64	30	-54	-32
						4.82	24	-72	-22
						4.26	16	-72	-22
	56.9	9.7	R	Area FG4	11.6	5.1	32	-50	-22
	33.4	5.7	R	AreaFG3	5.1	5.2	36	-40	-26
						4.72	40	-46	-26
	16.4	2.8	R	Area FG2	5	5.91	44	-58	-26
	12.6	2.2	R	Area FG1	5.1	6.04	34	-60	-20
	11.1	1.9	R	Lobule VIIa crusI (Hem)	0.3				
393	93.8	23.9	R	Lobule VIIIa (Hem)	12.8	4.36	28	-60	-52
	72.3	18.4	R	Lobule VIIIb (Hem)	10				
	59.7	15.2	R	Lobule VIIb (Hem)	9	5.39	28	-64	-52
						4.82	26	-66	-50
						4.61	24	-68	-48
	57.4	14.6	R	Lobule VIIIa (Verm)	27.1	4.6	6	-72	-38
						6.13	10	-72	-44
	32	8.2	R	Lobule IX (Hem)	4.5	5.03	16	-56	-46
						4.55	14	-54	-50
	11.2	2.9	R	Lobule VIIb (Verm)	34	4.92	0	-76	-34
390	348.5	89.4	L	Lobule VI (Hem)	18.6	5.57	-26	-68	-24
						4.91	-32	-52	-30
						4.64	-36	-46	-28
						4.59	-34	-48	-26
						2.91	-24	-50	-24
	16	4.1	L	AreaFG3	1.9				
	10	2.6	L	Lobule VIIa crusI (Hem)	0.3	5.48	-44	-54	-30
						4.73	-38	-52	-34
262	111.5	42.6	L	Lobule VIIIa (Hem)	14.6	6.81	-8	-72	-46
						4.89	-28	-52	-50
						5.41	-22	-60	-48
	72.4	27.6	L	Lobule VIIIb (Hem)	11.9				
	27.1	10.4	L	Lobule VIIb (Hem)	4	5.69	-20	-72	-48
						5.65	-22	-70	-46
						5.49	-22	-66	-44

Sleeve AND NoSleeve, pFWE<0.05, t>4.5									
1742	418.1	24	L	Lobule VIIa crusI (Hem)	13.8	7.09	-36	-64	-30
						7.07	-40	-64	-32
	338.8	19.4	L	Lobule VI (Hem)	18.1	7.02	-8	-76	-28
						6.87	-6	-78	-24
						6.22	-30	-58	-30
	194.6	11.2	L	Lobule VIIIa (Hem)	25.6	6.73	-8	-72	-46
	179.3	10.3	L	Lobule VIIb (Hem)	26.4				
	52.5	3	R	Lobule VIIb (Hem)	8	6.09	30	-64	-50
	51.4	2.9	L	Lobule VIIa crusII (Hem)	3.1				
	37.4	2.1	L	Lobule VIIIa (Verm)	25.3				
	32.5	1.9	R	Lobule VIIIa (Hem)	4.5				
	31.9	1.8	L	Lobule VI (Verm)	15.2				
	29.6	1.7	R	Lobule VIIIa (Verm)	14.1	6.06	10	-72	-44
	27.6	1.6	L	Lobule VIIb (Verm)	90.2	5.93	-22	-70	-44
	24.1	1.4	R	Lobule VI (Verm)	10.4				
	22.6	1.3	L	Lobule IX (Hem)	3.6				
	20.1	1.2	L	Lobule VIIIb (Hem)	3.3				
	16.1	0.9	R	Lobule VI (Hem)	0.9				
	13.8	0.8	L	Area FG2	2.7				
	13.3	0.8	R	Lobule VIIa crusII (Hem)	0.9	6.33	-44	-58	-28
	10.3	0.6	R	Lobule VIIb (Verm)	31.3				
593	307.8	51.9	R	Lobule VI (Hem)	17.1	6.86	28	-64	-24
						6.37	36	-46	-32
						5.68	32	-54	-34
						5.5	24	-76	-20
	178.4	30.1	R	Lobule VIIa crusI (Hem)	5.5	5.67	38	-62	-30
	33.3	5.6	R	Area FG2	10.2	5.99	40	-68	-22
						5.88	44	-60	-26
	29.3	4.9	R	AreaFG3	4.5	5.42	36	-40	-28
	25.3	4.3	R	Area FG1	10.2	5.98	34	-60	-20
	11.3	1.9	R	Area hOc4v [V4(v)]	1.8	6.23	36	-74	-22
Sleeve AND NoSleeve, masked with Exp. #1-3 pFWE<0.05, t>3.9									
321	237.1	73.9	R	Lobule VI (Hem)	13.1	6.95	28	-64	-24
						5.83	34	-46	-32
						5.64	30	-54	-32
						4.82	24	-72	-22
						4.26	16	-72	-22
	27	8.4	R	AreaFG3	4.1	5.2	36	-40	-26
						4.72	40	-46	-26
	21.9	6.8	R	Area FG4	4.5	5.1	32	-50	-22
	16.4	5.1	R	Area FG2	5	5.91	44	-58	-26
	10	3.1	R	Lobule VIIa crusI (Hem)	0.3				
210	93.4	44.5	L	Lobule VIIIa (Hem)	12.3	6.81	-8	-72	-46
						5.41	-22	-60	-48
	44	21	L	Lobule VIIIb (Hem)	7.3	5.69	-20	-72	-48
					4	5.65	-22	-70	-46
						5.49	-22	-66	-44
	27.1	12.9	L	Lobule VIIb (Hem)		4.89	-28	-52	-50
127	38.3	30.1	R	Lobule VIIIa (Verm)	17.9	6.13	10	-72	-44
						4.6	6	-72	-38
	26.4	20.8	R	Lobule VIIIa (Hem)	3.6	4.36	28	-60	-52
	26.3	20.7	R	Lobule VIIb (Hem)	3.9	5.39	28	-64	-52
						4.92	0	-76	-34
						4.82	26	-66	-50
						4.61	24	-68	-48
70	52.4	74.8	L	Lobule VI (Hem)	2.8	4.91	-32	-52	-30
						4.64	-36	-46	-28
						4.59	-34	-48	-26
66	64.4	97.5	L	Lobule VI (Hem)	3.4	5.57	-26	-68	-24
15	11.4	75.8	R	Lobule IX (Hem)	1.6	5.03	16	-56	-46
						4.55	14	-54	-50

Supplementary Figures

Supplementary Fig. 1: Effect of different analysis pipelines on cerebellar activation to action observation. (A-D) Cerebellar activations (p_{FWE}<0.05) for the four pipelines displayed on flat maps of the cerebellum. Color code in (A) identifies the different cerebellar lobules (Diedrichsen and Zotow, 2015). **(E)** For each of the four pipelines (A-D), the graphs shows the mean top 5% of t-values, and indicates the significant differences between the traditional pipeline (A) and the other three (B-D). *p<0.002, **p<0.001, ns=not significant. **(F)** As in (A) on the uncolored flat-map and on a sagittal slice. When smoothing is applied, the cerebellar cluster marked with the black arrow is part of a temporal lobe cluster. When smoothing is not applied as in (G) the cluster is clearly cerebellar. **(G)** Same as in (A) and (F) but computed on unsmoothed data. See Supplementary methods 1.1 and Supplementary results 1.1 and 1.2 for additional details.

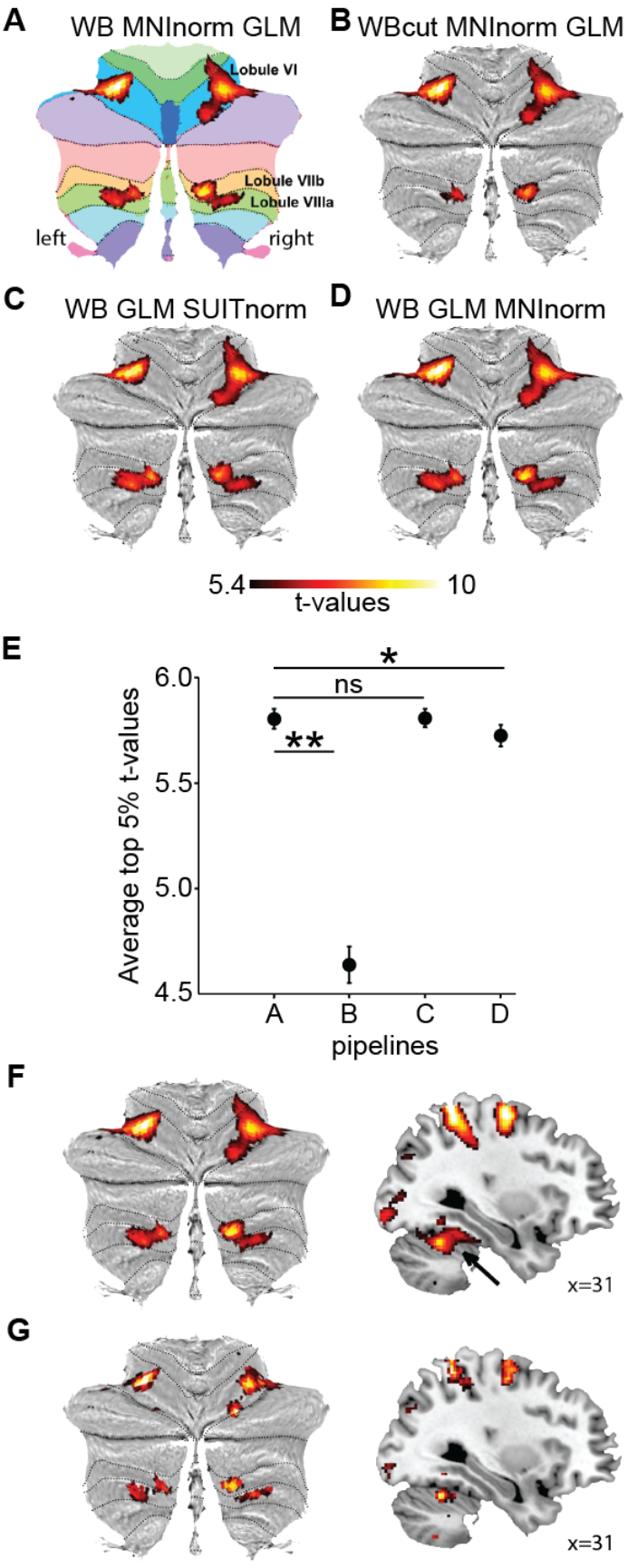

Supplementary Fig. 2: Cerebellar activity as a function of condition and lobule. Using Marsbar, for each of the 79 participants (combining experiments 1-3) we averaged the parameter estimate for ActionObs and CtrlObs across all the voxels of the four lobules separately for the right and left hemisphere. The figure then shows the mean and 95% credibility interval of these values based on a repeated measurement Bayesian ANOVA that included condition, lobule and hemisphere as factors of interest, and experiment as a factor of no interest. We then tested each distribution against zero (blue symbols) and across the two conditions (red symbols). Results confirm that lobule V did not respond to either conditions, while all other lobules discriminated conditions. A Bayesian was used to also provide evidence for the absence of activity in lobule V.

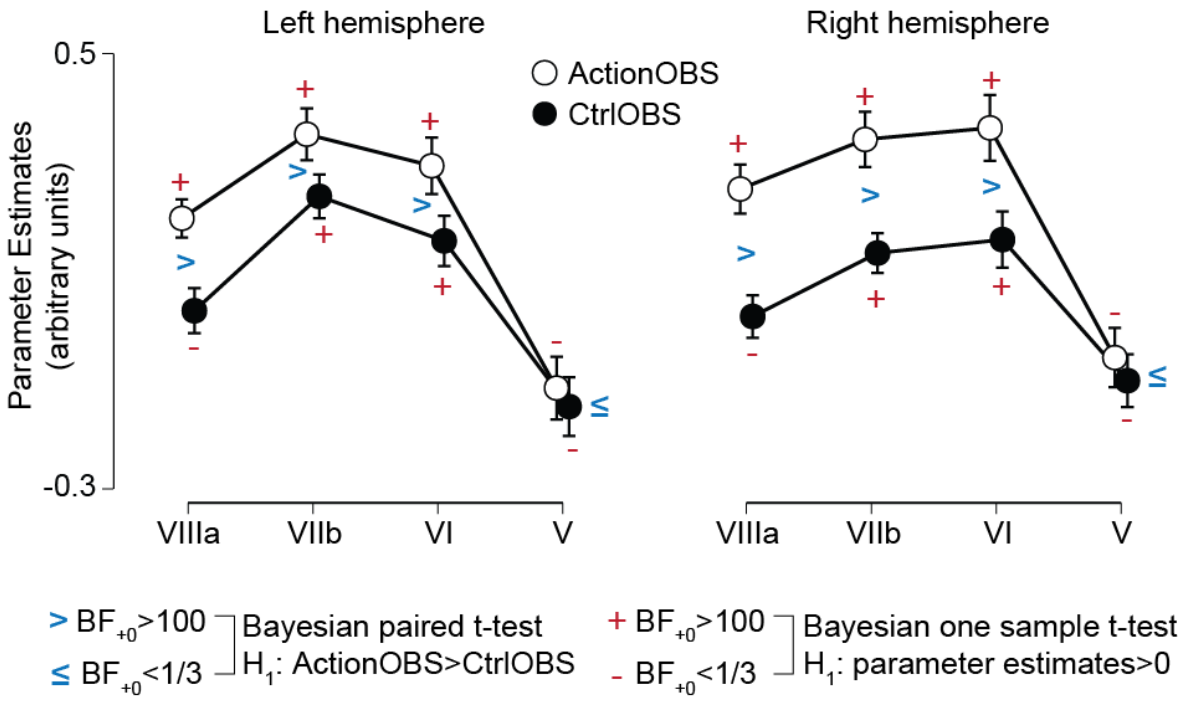

Supplementary Fig. 3: **Task-related eye movement dynamics. (A, B)** Heatplots based on spatial gaze intensity, identifying IRs during arm movement in the task for each group per condition. Both controls and SCA6 subjects focused significantly on the proximal arm muscles in the NoSleeve condition, although they focused on both distal and proximal part of the arm in the Sleeve condition, with an IR around the wrist. **(C)** Gaze position along the vertical axis throughout the task, showing tracking of upward going arm movements for both groups during both conditions. **(D)** Gaze position along the horizontal axis shows proximal arm focusing during arm movements in the NoSleeve condition. **(E, F)** Total gaze distance in the Sleeve condition along the V and H axis, respectively, shows no group differences. **(G, H)** Total gaze distance in the Nosleeve condition along the V and H axis, respectively, also shows no difference between groups.

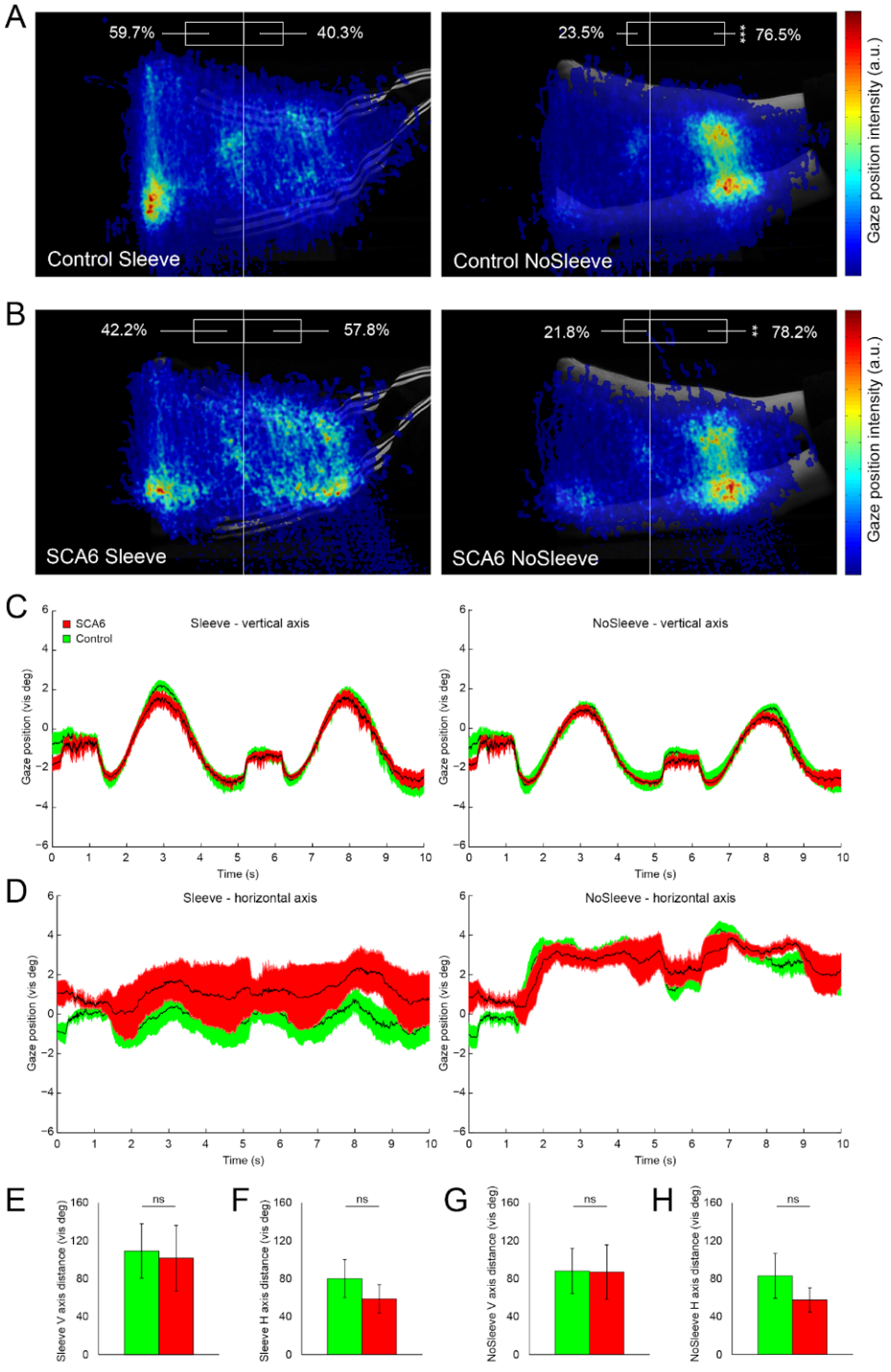

Supplementary Fig. 4. EMG recordings. For n=10 subjects (6 males; 9 right handed, mean age 32.5yrs, SD=4.3, range=29-42), we recorded EMG activity from the first dorsal interosseous (FDI) muscle of the right hand (using disposable, self-adhesive, wet gel electrodes with the ground electrode on the wrist and the other two electrodes as in the figure), which is involved in grasping, while participants watched 13 blocks of ActionObs and 13 blocks of ActionCtrl movies, as in experiments 1-3. Recordings were performed using a Biopack system (MP36, Biopac Systems Inc., Goleta CA, USA), and band-pass filtered (30-500Hz). To be as close as possible to the original fMRI condition, the recordings were performed in a mock MRI scanner to ensure a similar body position and screen projection size. EMG was quantified per block, as the surface under the rectified EMG signal. The boxplots show the quartiles of the EMG activity for each participant and condition. Analysing the results in a 2 Condition x 13 Repetition repeated measurement ANOVA using both frequentist and Bayesian analysis confirmed that there was no difference in EMG across the conditions (BF10=0.1 is strong evidence for the absence of a difference). Differential activity during the observation of these conditions in the MRI experiments in regions involved in motor control thus are unlikely to originate from differential covert imitation.

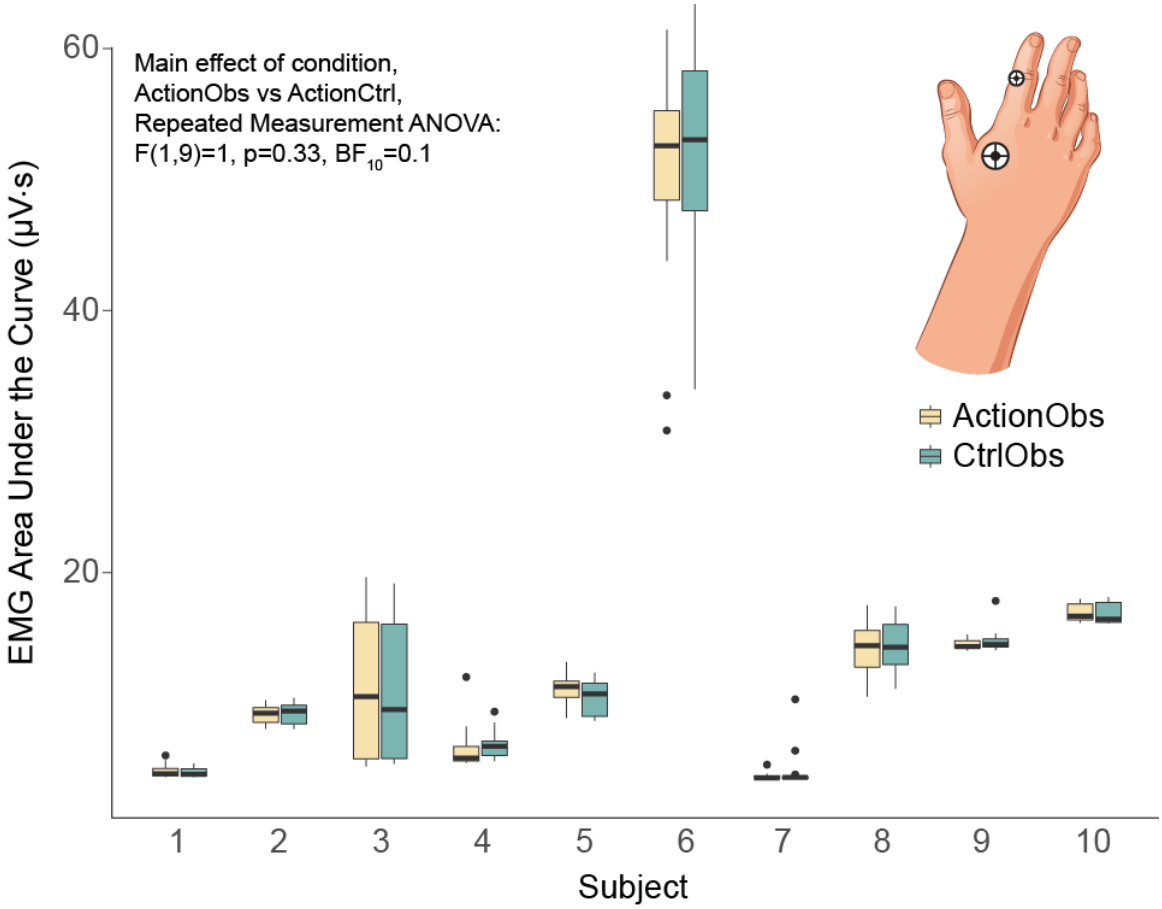

Supplementary Fig. 5: **Comparison with locations of VBM changes and eye movement cerebellar activity**. Red: location of cortical and cerebellar activity during eye movement tasks as identified by a Neurosynth (http://neurosynth.org/) meta-analysis with the term 'eye movements' (116 studies and 5486 activation clusters identified). The map is thresholded at $p_{FDR}<0.01$. Blue: cerebellar activation maps of the global null conjunction at pFWE<0.05 of the Sleeve and NoSleeve conditions falling within the conjunction of the ActionOBS-ActionCtrl contrasts of Exp.#1,2 and 3. From top to bottom, the coordinates (and blue crosses when present) indicate the location of: the left (top row) and right (middle row) lobule VI peak of correlation between VBM and SCA6 patients' performance in the Grooved Pegboard (from Table 3 in (Rentiya et al., 2017)), and (bottom row) the lobule VI peak of activity to eye movements as identified by the met-analysis in Neurosynth. Note how the VBM results (crosses) associated with SCA6 overlap with the regions recruited by our task (blue) but fall lateral to the regions most involved in eye movements (red). L: left hemisphere. R: right hemisphere. A: anterior. P: posterior. The clusters of activity are shown on the ch2better template from MRIcron (https://www.nitrc.org/projects/mricron/).

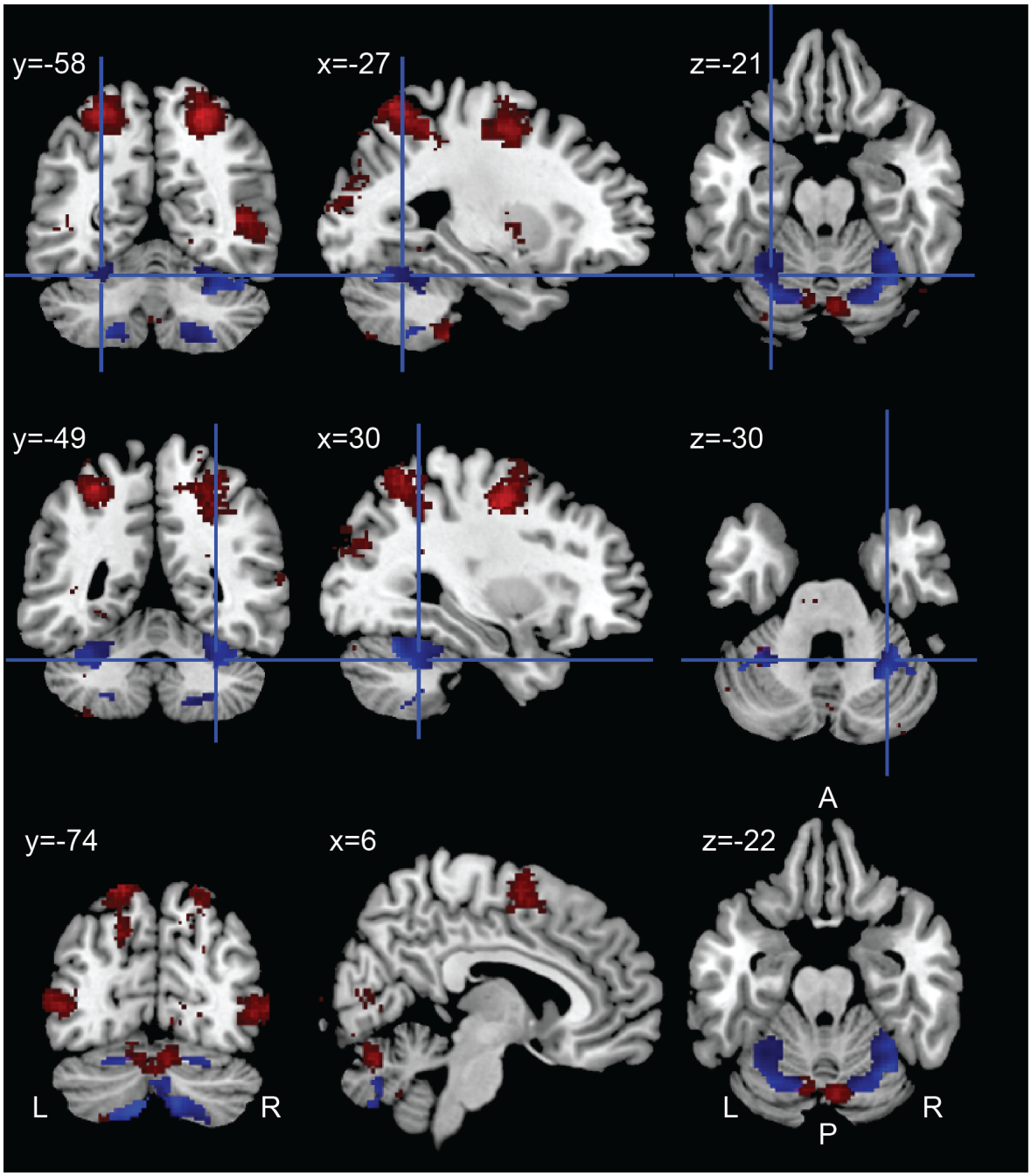

Supplementary Fig. 6: Effect of eye movements on visual cerebellar activity. (A) Activity for the ActionObs-CtrlObs contrast during the free viewing condition (as in Exp#1 to #3). (B) For visual comparison, the results of a global null conjunction between the results of Exp 1, 2 and 3. The bar graphs reflect the Action-Ctrl contrast for each of the 4 ROIs extracted using Marsbar. The letter under each bar refers to the panel in which the condition is illustrated (Free viewing, A; Fixation, C and Eye movements, D). The units of the contrast estimates on the Y axis are arbitrary. The error bars represent the s.e.m. across the 7 participants, a * that the contrast was significantly larger than zero at p_{unc}<0.05, ** at p_{unc}<0.01 (C) Same as A, but while participants were instructed to fixate on a red cross placed close to the object in the movie to suppress eye movements. (D) Same as A, but while participants simply followed a blue dot on a black screen that moved like the gaze of a free-viewing participant. (E) Activity during ActionEyeM against baseline, (F) same for CtrlEyeM. (G) Result of a meta-analysis using the search term 'Eye Movement' in Neurosynth as in Supplementary Figure 5. Because the minimum t-value showed in the flatmaps varies across contrasts, but the maximum was always set at 8, 't-threshold' in the color bar refers to this variable critical t threshold as indicated under each flatmap. Screen frames at the bottom of each panel describe the general design of a block for that experiment. As panel D-F come from the same experiment a single block example is shown. ITI=inter stimulus interval. See Supplementary methods 1.4 and Supplementary results 1.4 for further details.

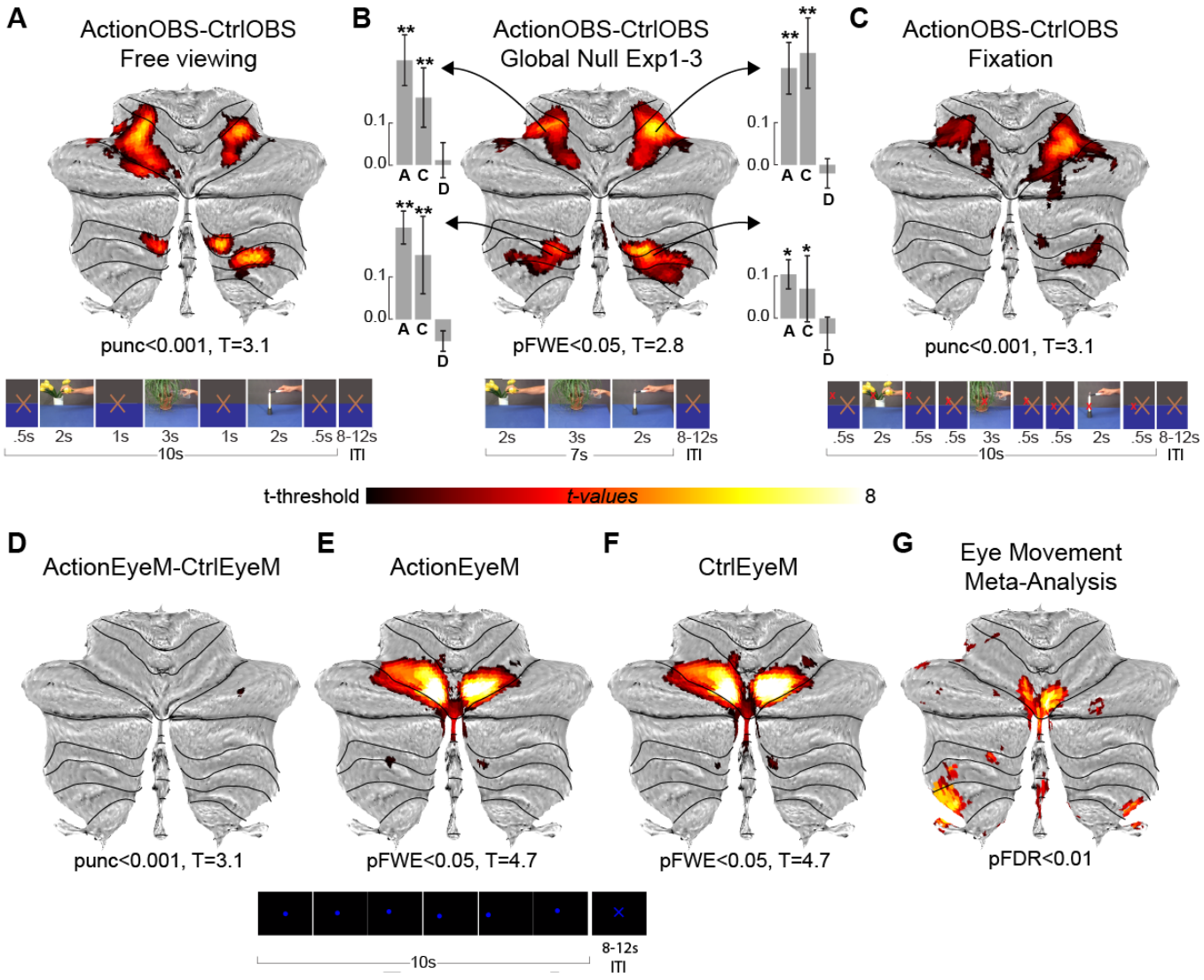

Supplementary Fig. 7: **Cortical activity to ActionOBS-CtrlOBS.** The activation maps show the results of the global null conjunction over the three action-observation experiments (Exp.#1-3) for the contrast ActionOBS-CtrlOBS. Maps are visualized on the SPM12 surface render (cortex_20484.surf.gii).

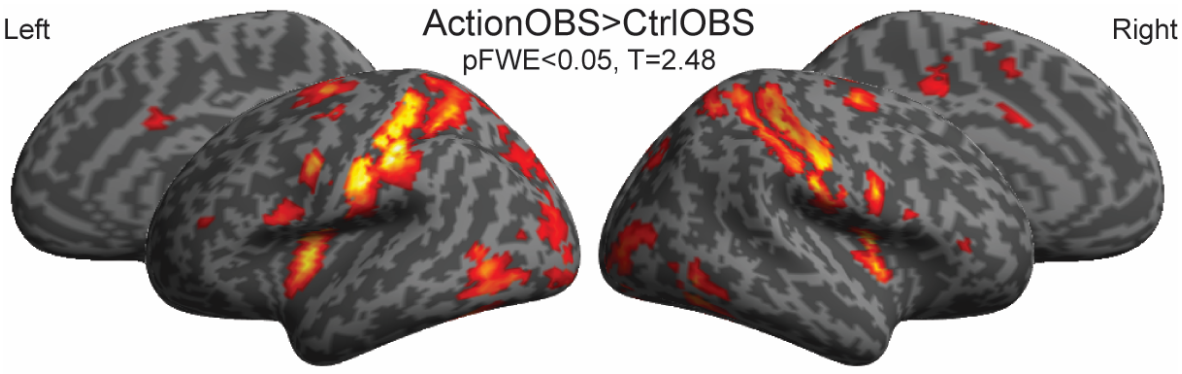

Supplementary Fig. 8: **Thalamic activity to ActionOBS-CtrlOBS. (A)** Brain activity to the ActionOBS-CtrlOBS contrast across Exp1, 2 and 3 (One-sample t-test GLM), shown at pFWE<0.05 (t=5.1). The red rectangle helps highlighting the location of the Thalamic activations. The clusters of activity are shown on the ch2better template from MRIcron (https://www.nitrc.org/projects/mricron/). **(B)** For each of the 79 participants (combining experiments 1-3) we averaged the parameter estimate for the ActionObs-CtrlObs contrast across all the voxels of the seven Thalamic ROIs, separately for the right and left hemisphere. The figure then shows the mean and 95% credibility interval of these values based on a repeated measurement Bayesian ANOVA that included hemisphere and ROI as factors of interest, and experiment as a factor of no interest. We then tested each distribution against zero with Bayesian one-sample t-test (H_1: ActionOBS-CtrlOBS>0). BF_{+0} values are indicated above each point.

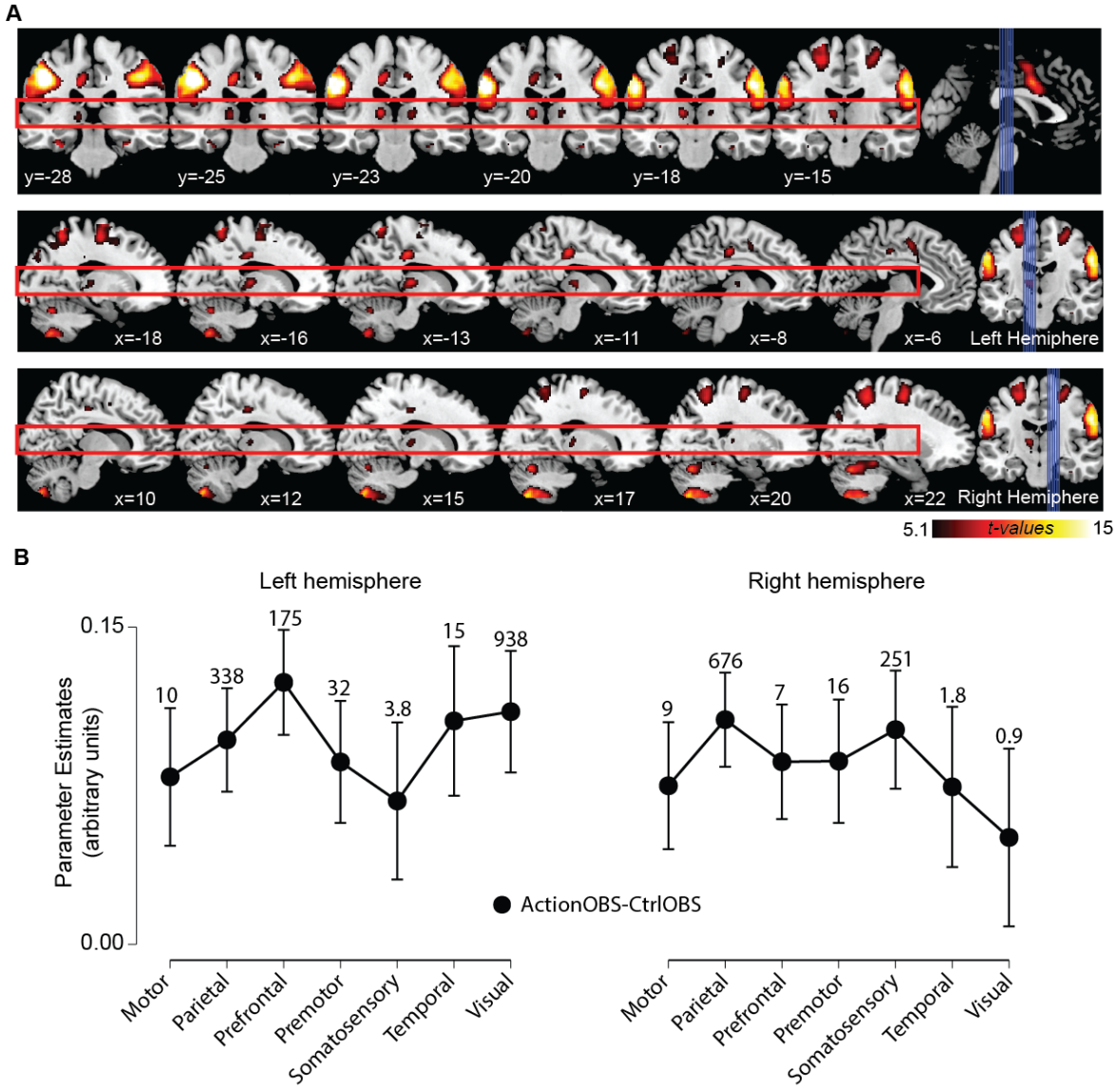

Supplementary materials and methods

Supplementary method 1.0. Recruitment procedure

The SCA6 patient group was recruited in collaboration with the department of Neurology at the Erasmus University Medical Center Rotterdam. A number of SCA patients had been approached by their physician for participating in a previous research project. As such, we built a database with names and addresses of volunteers that were willing to participate in research. Several volunteers approached our contact person individually and they were added to the database. Moreover, several participants were member of the Dutch society for Autosomal Dominant Cerebellar Ataxia (ADCA; www.ataxie.nl). Twenty-nine healthy control participants were recruited as relatives or friends of SCA patients or investigators, and were selected based on their age and gender to match the SCA patient group. All participants received an information letter or email asking whether they were interested in participating in the study.

Supplementary method 1.1. Impact of different analysis pipelines

Four pipelines were computed and compared to test the effect of different spatial normalization procedures. The analyses were done in SPM8 (Wellcome Trust Centre for Neuroimaging, UCL, UK) and complemented with customized Matlab scripts (Matlab 7.14; The MathWorks Inc., Natick, USA). Common to all, data pre-processing included: slice time correction of functional images using the bottom slice, located in the posterior cerebellum, as a reference slice; realignment and co-registration of the T1-weighted anatomical to the mean functional image. Below a description of the steps that followed for each pipeline separately. Supplementary Table 2 more schematically illustrates the analysis steps used for the four pipelines. For Exp. #1, the acquisition plane was tilted by 30-45° from the AC-PC plane to cover the entire cerebellum.

Pipeline I: WB_MNInorm_GLM. As commonly done in fMRI analyses, the whole brain (WB) functional images were brought to MNI space before computing the GLM, using the normalization (norm) parameter generated during segmentation of the anatomical image (final voxel size: 2 × 2 × 2 mm). We manually adjusted the SPM8 bounding box settings to [-90 -126 -72; 91 91 109] to cover the entire cerebellum.

Pipeline II: WBcut_MNInorm_GLM. Same as for Pipeline I but without adjustment of the bounding box, which was left to the default SPM8 settings [-78 -112 -50; 78 76 85]. This allowed us to identify which part of the activation was left out in previous studies focusing on the cortex.

Pipeline III: Cereb_GLM_SUITnorm. A template for cerebellar-specific normalization using a high-resolution atlas of the human cerebellum (Cereb) is available in the literature (SUIT, Diedrichsen, 2006; Diedrichsen *et al.*, 2009), and it has been shown to improve the alignment of anatomical landmarks and increase average t-values for cerebellar functional data sets (Diedrichsen, 2006). The SUIT template is in MNI space, but it is based on a group of 20 participants in order to create an average anatomical template with enough anatomical details to account for the small size of cerebellar functional regions(Diedrichsen, 2006). In pipeline III, following the method suggested by (Diedrichsen, 2006), after co-registration, the functional images were directly fed into the subject-level general linear models. Resulting contrast images were subsequently normalized to the SUIT-space, by first isolating the cerebellum from the T1 images using an automated algorithm from the SUIT toolbox (www.icn.ucl.ac.uk/motorcontrol/imaging/suit.html). This step resulted in a cropped anatomical image covering the cerebellum and adjacent cortical regions, which was normalized into SUIT cerebellar space. The transformation parameters obtained during the normalization were then used to normalize the contrast images resulting from the first level GLM (final voxel size: 2 × 2 × 2 mm).

Pipeline IV: WB_GLM_MNInorm. The Cereb_GLM_SUITnorm pipeline differs from traditional whole brain pipelines not only in the normalization template but also in the moment at which normalization is computed: after vs. prior to the GLM. In order to assess the impact of this difference, pipeline IV was run with the same temporal order used in pipeline III: the first level GLM used the co-registered functional images, and the normalization to the MNI whole brain template was applied on the contrast images resulting from the GLM. Normalization parameters were calculated during the segmentation of the whole-brain T1 anatomical image (final voxel size: 2 × 2 × 2 mm). In order to include the entire cerebellum, the bounding box was manually adjusted to [-90 -126 -72; 91 91 109].

Smoothing, using a 6 mm FMHW Gaussian kernel, was applied to each pipeline after normalization. Although spatial smoothing is routinely applied in the neuroimaging literature, it poses the possibility of leakage of

activation between the anterior cerebellum and the temporal cortex. We therefore report our results with and without the 6 mm FMHW Gaussian filter for our WB_MNInorm_GLM pipeline, which is closest to traditional MRI analysis in the literature. The impact of smoothing on leakage between cortical and cerebellar activation is also investigated by comparing cerebellar activity resulting from whole brain analyses run on either smoothed or unsmoothed data.

The same general linear models was applied to each pipeline. Two standard box car predictors modelled the ActionOBS, CtrlOBS and static conditions, and were convolved with the canonical hemodynamic response function (HRF). The last six regressors of no interest included the displacements and rotations determined during image realignment. The ActionOBS-CtrlOBS contrast was computed at the subject-level to generate action specific activations for observation, and tested against zero with a one-sample t-test at the group level. The static condition was modelled at the first level, but for the purpose of this study, not analyzed at the second level.

The choice of the statistical threshold at which to report the group results is not trivial. First, we want to be able to compare multiple activation maps resulting from different preprocessing pipelines. Second, correction algorithms based on random field theory require a certain amount of smoothness (Brett et al. 2004), which is not given using unsmoothed data sets. All statistical maps thus are thresholded at $p_{FWE}<0.05$ and have minimal cluster size of 10 voxels. We chose peak-level FWE-correction because we wished to (i) interpret activation of individual voxels, and, motivated by the inconsistencies of cerebellar activations in the literature, (ii) limit the risks of Type I errors.

Anatomical descriptions of cerebral activity were guided by the probabilistic cytoarchitectonic maps (Geyer *et al.*, 1996, 1999, 2000; Amunts *et al.*, 1999; Grefkes *et al.*, 2001; Geyer, 2004; Eickhoff *et al.*, 2005, 2006; Caspers *et al.*, 2006; Choi *et al.*, 2006) implemented in the anatomy toolbox for SPM (http://www.fz-juelich.de/ime/spm_anatomy_toolbox) (Eickhoff *et al.*, 2005, 2006, 2007).

To investigate the impact of different pipelines, we used unsmoothed contrast images resulting from the 1st-level analysis of action observation data after setting them to identical image dimensions (91 × 109 × 91) using the ImCalc function. The contrast images were then fed to group-level, one-sample t-test, GLM models (ActionOBS-CtrlOBS>0), one for each pipeline. Voxels missing in any of the four pipelines were excluded for the analysis with exception of the voxels missing due to the bounding box size, which were coded with 0, such that differences between the pipelines could also be evaluated in the inferior posterior cerebellum. The t-values from the four group-level t-values cerebellar maps were summed up using the NIfTI toolbox (version 1.25). In line with (Diedrichsen, 2006), in order to compare the results of the four pipelines without biasing the comparison a priori to any specific pipeline, we selected from the sum of the four t-maps, the location of the 5 percent of voxels with the highest t-value sums as voxels of interest. The pipelines were then compared using a repeated-measures ANOVA design that considers each voxel of interest as a 'subject', and each pipeline a repeated measurement of this 'subject' (i.e. voxel). We then planned to perform t-tests that compare each of the pipelines against the WB_MNInorm_GLM pipeline, because the whole brain analysis is most frequently used in the neuroimaging literature.

Supplementary method 1.2. Consistency maps

To generate the consistency maps, the normalized, smoothed single-subject t-maps of action observation (ActionOBS-CtrlOBS>0) from Exp.#1-3 were thresholded at the t-value corresponding to $p_{unc}<0.001$ (T=3.1), which binarizes the images. All single-subject maps were then added together to generate the group-level consistency map, showing for each voxel the number of participants for which the voxel was significantly activated by action observation. The number of participants needed to show that a voxel is activated more consistently than expected by chance, was calculated using a cumulative binomial distribution with 31 repetitions and an associated probability of 0.001. The resulting probability was Bonferroni corrected using the number of voxels in the search volume (170675 for the whole brain). Thus, a voxel activated by four or more participants can be considered above chance (Gazzola and Keysers, 2009).

Supplementary method 1.3. Eye-tracking data acquisition and analysis

Eye tracking measures of 4 patients (mean age 60.4y ± 10.6 SD; mean SARA score: 10.88 ± 8.37 SD) and 7 control participants (mean age 63.5y ± 5.7 SD) were collectedduring the weight discrimination task using the EyeLink® 1000 system (SR Research Ltd., Mississauga, Ontario, Canada) at 500Hz. Participants sat up

straight behind a desk and kept their head placed on a Head Support (SR Research Ltd., Mississauga, Ontario, Canada), providing support for the chin and forehead during the entire task. Task stimuli were presented using PsychoPy2 (v1.84, UON, UK)(Peirce, 2009) on a 19 inch TFT monitor (UltraSharp 1907FP, Dell, TX, USA) with 300x380cm dimensions, a resolution of 1280x1080 pixels and at a refresh rate of 55Hz. Distance between participants' eyes and screen was 593 ± 22.8 mm and room background light was minimized during the task. The presented clips appeared in the middle of the presentation screen and covered 720x480 pixels. A 9-point calibration and validation was executed before starting the experiment. PsychoPy2 sent text messages to be registered in EyeLink at the beginning and end of each pair of clips for synchronization purposes.

EyeLink EDF files were converted into MATLAB-compatible (MathWorks, USA) variables using the 'edf2mat' script (JN van der Geest, Dept of Neurosci, Erasmus MC, Rotterdam) and were further analysed using custom-written MATLAB code. Data was obtained on eye-related events (i.e. blinks, fixations and saccades) by using default gaze parser settings (EyeLink 1000 User's Manual, SR Research, Ontario, Canada). Data was filtered using a Gaussian lowpass filter with a 50Hz cutoff frequency and was converted from pixels to visual degrees, using X and Y resolution values as calculated by EyeLink. We synchronized eye movement recordings with start of each pair of clips based on message event timestamps corresponding to start of the pair of clips. Then, for each clip we visually determined periods in which object lifting-associated arm movement occurred and we quantified eye-related parameters of events occurring during those periods, comparing SCA6 patients and controls. Parameters included number of saccades, blinks and fixations, duration of blinks and fixations (in milliseconds), saccade peak velocity (in visual degrees/second), saccade amplitude (in visual degrees) and distance in the horizontal and vertical plain (calculated on trial basis during 'fixation periods', representing smooth pursuit and drift). All of these parameters were calculated based on clip periods where arm movement occurred. To make a distinction between distal and proximal part of the arm, we decided on a x-coordinate (pixel 380 from left side movie) based on movies where a arm without sleeve was visible. We took into account arm movement dynamics during the movie and attempted to encompass deformations of the brachior radialis muscle during lifting in the proximal part of the arm (right side of the movie) and movements of the hand and wrist in the distal part of the arm (left side). The same x-coordinate was used for every movie analysed in both Sleeve and NoSleeve conditions.

Heat plots (Supplementary Fig. 2A, B) were generated based on matrices where values represented summation of gaze positions for each datapoint *during the period of arm movement*, separating Sleeve versus NoSleeve conditions. Matrices were processed using a 2-D circular averaging filter with a radius of 3 in replicate boundary setting, converted into a grayscale image and thresholded using an alphamask, so that values higher than 0.002 (on a scale of 0-1) were plotted with 75% opacity using colormap 'jet' on top of a two merged representative frames from movies in the Sleeve and NoSleeve conditions, showing begin and end-position of a lift movement. Gaze position over time was calculated from gaze positions in the V and H axis of all subjects per group (Supplementary Fig 2C, D). Distance along both axis was calculated by summation of the absolute difference between sampling points during the task (Supplementary Fig. 2E - H). Figures were further processed in Illustrator CS6 (Adobe, USA).

The different eye tracking measures of patients and controls have been compared using pairwise independent two sample t-tests. While not being a prominent feature, previous studies have found abnormalities in saccades for SCA6 patients (Gomez *et al.*, 1997; Buttner *et al.*, 1998; Christova *et al.*, 2008), based on this a priori hypothesis we have performed one-tailed tests for all saccade metrics. We have used FDR correction as a more lenient multiple comparisons correction method as opposed to the more conservative Bonferroni correction, to increase our sensitivity to group differences.

Eye tracking measurements have been performed on a subset of patients and controls, to check whether these subsets are representative for their respective groups we performed the main Group analysis on task performance. There were no significant performance differences between controls and their eye tracker subgroup [$F(1,36) = 0.6655$, $p > =0.420$, $w2 = 0.0038$] nor between patients and the eye tracker patient subgroup [$F(1,22) = 1.3605$, $p =0.256$, $w2 = 0.0097$].

Supplementary method 1.4. The effect of eye movements

The logic of this fMRI control experiment participants was to explore whether the differential cerebellar activity for ActionObs-CtrlObs could be reduced to differential eye movements between these conditions. We aimed thus to disentangle the contribution of the movies from those of the eye movements triggered by the movies, by comparing brain activity in three conditions.

(i) Free viewing. Participants watched the same ActionOBS and CtrlOBS stimuli as in Exp. #1 to 3 freely, without any particular instruction. The only difference with the structure of the task in Exp. #1 to 3 is that a baseline 1s fixation cross was inserted between the videos of each block (Supplementary Fig. 6A). This was done in order to match the block design to the Fixation condition. All the rest was kept the same as in Exp. #1 to #3. Participant's eye movements are therefore free and spontaneous.

(ii) Fixation. Participants watched the same ActionOBS and CtrlOBS stimuli while fixating on a red cross superimposed on each movie (Supplementary Fig. 6C). The red fixation cross remained stationary for the duration of each movie clip within the block and was placed at a location near the objects such that the action could been seen well without moving the eyes. This red fixation cross was presented 500ms before each clip started and stayed there for an additional 500ms after the movie. This was done to ensure that the eyes are already at the fixation before the movie started and that there a no erratic eye movement during the presentation of the movie. As the location of the objects varied between clips, the location of the cross therefore differed for each movie. The experimenter controlled in real-time, via the eye tracking camera that participants indeed followed the instructions to suppress eye movements during this condition.

(iii) EyeMovements. We recorded the eye movement of a volunteer, not taking part in the fMRI experiment, while he viewed the ActionObs and ActionCtrl stimuli of the free viewing condition. This was done while he laid in the scanner, to ensure all the eye movement conditions remain similar. Using the eye-gaze data, we then generated movies that had a black background, and a blue dot where that participant's gaze had been moment by moment (Supplementary Fig. 6D). This generated 26 movies: 13 ActionEyeM and 13 CtrlEyeM movie. Participants were then instructed to simply follow the blue dot, so as to generate a pattern of eye movements similar to that during free viewing of the two ActionOBS and CtrlOBS conditions without seeing the actual actions.

Seven new participants (5 females, 2 males, M_{age} = 26 years, SD 4.5) were recruited for the experiment (Table 1) and each performed 3 runs of fMRI data acquisition (one per condition). The Three conditions were manually randomized between the subjects.

fMRI data analysis: Pre-processing and modelling was performed as in experiment 1, except that the data of the 7 participants was modelled at the first level as if they were 7 runs from the same participants in a single first level (fixed effect) model. This was done because with so few participants, a random effect model would have been underpowered. Data is shown on cerebellar flatmaps using a threshold of $p<0.001$ uncorrected. Using the same fixed effect model but with un-smoothed data, we also extracted the data from the 4 cerebellar ROIs identified from Experiments 1-3 using Marsbar to compare the Action-Ctrl contrast across the 3 conditions in the 4 ROIs. For this, Marsbar extracted the average activity across all the voxel of each ROI, and then performed a GLM using the SPM design matrix used for the voxel-wise analysis. We also extracted the contrast estimates for each participant separately, to generate a bar graph with error bars that reflect the s.e.m. across 7 participants, but the significance of the Action-Ctrl contrast was assessed using the fixed effect p-value, pooling the activity of all participants.

Supplementary Results

Supplementary results 1.1 Effect of different analysis pipelines on cerebellar activation during action observation

When we mapped the activations triggered by viewing goal directed hand actions compared to control stimuli (ActionOBS-CtrlOBS) with a traditional pipeline and a bounding box encompassing the whole cerebellum, we found four main clusters of activation. Supplementary Fig. 1A and Supplementary Table 3 locate these clusters in the bilateral Lobule VI, VIIIa and VIIb. When the smaller SPM8 default bounding box was used

the activations in Lobule VIIIa were not visible as they were not included in the search volume used in the analyses (Supplementary Fig. 1B).

Analyzing the data with the specific cerebellar normalization and the procedure proposed by (Diedrichsen, 2006; Diedrichsen *et al.*, 2009) results in the same clusters of activity identified with the traditional approach (Supplementary Fig. 1C and Supplementary Table 3). When the average top 5% of t-values is compared between the traditional and cerebellar specific pipeline (Supplementary Fig. 1E), no significant difference is observed between the two approaches ($p>0.95$, $t=-0.06$). Bayesian paired sample t-test confirms that there is evidence for the two pipelines to give equal results ($BF_{10}=0.043$; https://jasp-stats.org/). To investigate the impact of running the GLM in the subject space, instead of on normalized data, as it is done in the cerebellar optimized pipeline, we re-calculated the whole brain analysis following the same order of pre-processing. While at visual inspection the maps look very similar (Supplementary Fig. 1D), the top 5% t-values is significantly lower ($p<0.002$, $t=3.14$). Supplementary Fig. 1E also indicates a significant drop of t-values ($p<0.001$, $t=11.8$) when the small bounding box is used, likely due to part of the active voxels not included in the statistical computation.

In summary, these results indicate that as long as the whole cerebellum is included in the analyses, activations are preserved across different analysis pipelines. Additionally in our data set, no clear advantage is observed when using the pipeline optimized for the cerebellum compared to the traditional one, possibly due to improvement of co-registration and normalization algorithms in the newer SPM releases, which do not make the specific adjustments for the cerebellum anymore necessary.

Supplementary results 1.2 Effect of spatial smoothing on cerebellar activation during action observation

Because the dorsal cerebellum is located close to the ventral temporal lobe, one concern in reporting cerebellar activations from whole brain analyses is that smoothing could make activations of the ventral visual stream bleed into the cerebellum. Comparing results computed on unsmoothed and smoothed data indicates that spatial smoothing increases the number of super-threshold voxels during action observation (ActionOBS-CtrlOBS>0) in the cerebellum by 168%, from 350 to 939 voxels, given the same t-value threshold of t=5.8 (corresponding to the most stringent t value resulting from FWE of whole brain smoothed and unsmoothed results). However, smoothing caused clusters that are separated when using unsmoothed data to merge into a single cluster (arrow in Supplementary Fig. 1F). In particular, the merging happened within the right cerebellar lobule VI, and bilaterally between the cerebellar lobule VIIb and VIIIa. Results on the unsmoothed data confirm cerebellar activations in all previously identified clusters, including the dorsal lobule VI, supporting the notion that activations are not the result of smoothing leading to a bleeding of activation from ventral visual cortex onto the adjacent cerebellum (Supplementary Fig. 1G). Despite unsmooth results confirming the extensive cerebellar activation on the lobule VI, the cluster still belong to a bigger cluster encompassing the fusiform gyrus, making a clear attribution of voxels at the border to the fusiform or the cerebellum more difficult, which is evident in some of the tables. Additionally, 80% of the lobut VI cluster reported by (Van Overwalle *et al.*, 2014) falls within the fusiform regions (FG4 in particular), suggesting that smoothing might have had a bigger impact on the meta-analysis maps computation.

Supplementary results 1.3 Eye movements during the weight discrimination task

In the Sleeve condition, subjects from both groups focussed equally on the distal and proximal part of the arm (Ctrl: $t_{(12)}=1.523$, $p=0.154$; SCA6: $t_{(6)}=-0.802$, $p=0.453$; Supplementary Fig. 2A and B, left panels). In the NoSleeve condition both groups focussed significantly more on the proximal muscles of the lower arm (Ctrl: $t_{(12)}=-9.482$, $p<0.001$; SCA6: $t_{(6)}=-4.238$, $p=0.005$; Supplementary Fig. 2A and B, right panels). There was no group difference in either condition (Sleeve: $t_{(9)}=1.112$, $p=0.295$; NoSleeve: $t_{(9)}=-0.197$, $p=0.848$).

There were no significant group differences in any of the following parameters: number of saccades ($t_7= 2.17$, p-value= 0.197), Saccade peak velocity ($t_7= 2.32$, p-value= 0.197), saccade amplitude ($t_6= 1.45$, p-value= 0.327), duration of blinks ($t_5= -0.15$, p-value= 0.995), time lost blinking ($t_9= 0.33$, p-value= 0.995), duration of fixations ($t_6= 1.72$, p-value= 0.327), duration of fixation ($t_8= -1.6$, p-value= 0.327).

We next investigated whether the trajectory of eye movement over time differed across groups. (Supplementary Fig. 2C). We did not observe any differences between groups for the Sleeve (V: $t_{(9)}=0.163$,

p=0.874; H: $t_{(9)}$=0.727, p=0.486; Supplementary Fig. 2E and F) and NoSleeve condition(V: $t_{(9)}$=0.03, p=0.977; H: $t_{(9)}$=0.762, p=0.465; Supplementary Fig. 2G and H).

Supplementary results 1.4. The effect of eye movements.

Supplementary Figure 6 shows, that activity during Free Viewing in 7 participants (Panel A) replicates the results of the main experiments (Panel B), with significant differential activity in the ActionObs-ActionCtrl contrast visible bilaterally in lobule VI and VIIb and in the right lobule VIIIa. Minimizing eye movements using our fixation condition slightly reduces the activity in this contrast (Panel C), but differential activity remains clearly visible in bilaterial lobule VI, and in the right lobule VIIb/VIIIa. Guiding participants to perform eye movements similar to those during free viewing, but without the movies, however does not lead to significant activity in the cerebellar cortex for the ActionEyeM-CtrlEyeM contrast (Panel D). Indeed, if we extract the contrast values from the four ROIs of the main experiment (bar graphs in Panel B), we see that in all 4 ROIs the Action-Ctrl contrast is significant whenever participants view the action movies, be it while being free to move their eyes (Free viewing) and while their eye movements are discouraged (Fixation). In contrast, if they do not see the action movies, but lead to perform similar eye movements, the contrast is clearly non-significant. Finally, examining activity separately, while participants performed the eye movements similar to those while viewing action movies (ActionEyeM, Panel E) and those while viewing the control movies (CtrlEyeM, Panel F), we do observe activity in the cerebellum, but this activity is strongest in a location that is more medial than that in the ActionObs-ActionCtrl contrast, in line with where an eye movement meta-analysis using Neurosynth (Panel G) identifies consistent activity in papers related to eye movements. This activity is however so similar across the Action and Ctrl condition, that it disappears in the contrast.

In summary, this experiment suggests that the activity pattern identified in the cerebellum in experiments 1-3 is unlikely to be due to differential eye movements, because (a) it persists when eye movements are discouraged in our fixation condition and (b) because that difference is not significant while encouraging participants to replicate the eye-movements recorded during free viewing.

Supplementary References

Amunts K, Schleicher A, Bürgel U, Mohlberg H, Uylings HBM, Zilles K. Broca's region revisited: Cytoarchitecture and intersubject variability. J Comp Neurol 1999; 412: 319–341.

Buttner N, Geschwind D, Jen JC, Perlman S, Pulst SM, Baloh RW. Oculomotor phenotypes in autosomal dominant ataxias. Arch Neurol 1998; 55: 1353–7.

Caspers S, Geyer S, Schleicher A, Mohlberg H, Amunts K, Zilles K. The human inferior parietal cortex: Cytoarchitectonic parcellation and interindividual variability. Neuroimage 2006; 33: 430–448.

Choi HJ, Zilles K, Mohlberg H, Schleicher A, Fink GR, Armstrong E, et al. Cytoarchitectonic identification and probabilistic mapping of two distinct areas within the anterior ventral bank of the human intraparietal sulcus. J Comp Neurol 2006; 495: 53–69.

Christova P, Anderson JH, Gomez CM. Impaired Eye Movements in Presymptomatic Spinocerebellar Ataxia Type 6. Arch Neurol 2008; 65: 530.

Diedrichsen J. A spatially unbiased atlas template of the human cerebellum. Neuroimage 2006; 33: 127–138.

Diedrichsen J, Balsters JH, Flavell J, Cussans E, Ramnani N. A probabilistic MR atlas of the human cerebellum. Neuroimage 2009; 46: 39–46.

Diedrichsen J, Zotow E. Surface-based display of volume-averaged cerebellar imaging data. PLoS One 2015; 10

Eickhoff SB, Heim S, Zilles K, Amunts K. Testing anatomically specified hypotheses in functional imaging using cytoarchitectonic maps. Neuroimage 2006; 32: 570–582.

Eickhoff SB, Paus T, Caspers S, Grosbras MH, Evans AC, Zilles K, et al. Assignment of functional activations to probabilistic cytoarchitectonic areas revisited. Neuroimage 2007; 36: 511–521.

Eickhoff SB, Stephan KE, Mohlberg H, Grefkes C, Fink GR, Amunts K, et al. A new SPM toolbox for combining probabilistic cytoarchitectonic maps and functional imaging data. Neuroimage 2005; 25: 1325–1335.

Gazzola V, Keysers C. The Observation and Execution of Actions Share Motor and Somatosensory Voxels in all Tested Subjects: Single-Subject Analyses of Unsmoothed fMRI Data. Cereb Cortex 2009; 19: 1239–1255.

Geyer S. The microstructural border between the motor and the cognitive domain in the human cerebral cortex. AdvAnatEmbryolCell Biol 2004; 174: I–89.

Geyer S, Ledberg A, Schleicher A, Kinomura S, Schormann T, Burgel U, et al. Two different areas within the primary motor cortex of man. Nature 1996; 382: 805–807.

Geyer S, Schleicher a, Zilles K. Areas 3a, 3b, and 1 of human primary somatosensory cortex. Neuroimage 1999; 10: 63–83.

Geyer S, Schormann T, Mohlberg H, Zilles K. Areas 3a, 3b, and 1 of human primary somatosensory cortex. 2. Spatial normalization to standard anatomical space. Neuroimage 2000; 11: 684–696.

Gomez CM, Thompson RM, Gammack JT, Perlman SL, Dobyns WB, Truwit CL, et al. Spinocerebellar ataxia type 6: gaze-evoked and vertical nystagmus, Purkinje cell degeneration, and variable age of onset. Ann Neurol 1997; 42: 933–50.

Grefkes C, Geyer S, Schormann T, Roland P, Zilles K. Human somatosensory area 2: Observer-independent cytoarchitectonic mapping, interindividual variability, and population map. Neuroimage 2001; 14: 617–631.

Van Overwalle F, Baetens K, Mariën P, Vandekerckhove M. Social cognition and the cerebellum: A meta-analysis of over 350 fMRI studies. Neuroimage 2014; 86: 554–572.

Peirce JW. Generating Stimuli for Neuroscience Using PsychoPy. Front Neuroinform 2009; 2: 10.

Rentiya Z, Khan N-S, Ergun E, Ying SH, Desmond JE. Distinct cerebellar regions related to motor and cognitive performance in SCA6 patients. Neuropsychologia 2017; 107: 25–30.